Thermal Analysis of a Twin Screw Vacuum Pump using CFD Model

Sham RANE[1]*, Ahmed KOVAČEVIĆ[1], Khurram AKHTAR[2], Christopher WHITE[2]

[1]City, University of London, London, UK, EC1V0HB.
sham.rane@city.ac.uk, a.kovacevic@city.ac.uk

[2]Fruitland Manufacturing Vacuum pumps, Ontario, L8E 2N7, Canada.
kakhtar@fruitland-mfg.com, cwhite@fruitland-mfg.com

* Corresponding Author

ABSTRACT

Twin screw machines that are used in vacuum pump application have large wrap angle and length-to-diameter ratio in comparison to classical twin screw machines used in compressor applications. However, the compressor type asymmetric rotor profile with lower wrap angle can be re-designed such that the machine can switch its operation from medium pressure ratio above ambient to a vacuum operation from very low pressure to ambient i.e., high pressure ratio. This switching results into a high heat generation rate within the rotors and demands for additional cooling measures in the rotor design. In this study, CFD model of a 3-5 Twin screw vacuum pump was used to evaluate the thermal performance of the machine. SCORG grid generator and ANSYS CFX solver were used for setting the model. Experimental observations related to inefficient heat dissipation on the intake of the rotors were analysed for its causes and potential design solutions. Air injection for cooling in the current configuration was evaluated and impact of design modifications was estimated using this CFD model. The developed model will be further used to redesign the high-pressure ports and air injection system to improve the thermal cooling effectiveness and specific power of the machine.

1. INTRODUCTION

In the presented study, a patented screw vacuum pump technology, (Akhtar and White, 2023), has been evaluated. This twin screw vacuum pump uses a conventional asymmetric 'N' rotor profile of synchronised dry-air twin screw compressor and special cooling ports for application to vacuum. In some previous studies, the computational model for positive displacement machines such as twin-screw compressors has been described in Kovačević (2005, 2007) and is widely applicable. Rane (2017a, 2017b, 2021a) and Kovačević (2017) have presented the development and application of different types of deforming grid topologies that can be used for modelling of twin-screw machines. Applications to dry air and oil injected compressors and ORC expanders have been investigated. A bi-directional coupling of fluid flow and structural solvers was reported by Rane *et al*. (2021b). The application was for a dry air twin-screw compressor. Conjugate heat transfer (CHT) model was used to produce boundary conditions required for the structural solver that evaluated the local leakage gap variation, in turn this was supplied to the CFD – CHT model to update the flow field. Studies for Roots blower type of CFD model indicate that the deforming rotor grid is a critical element of the setup as it directly controls the interlobe and radial gap sizes. Additionally, the rotor profiles could have special tip design which can result into local flow features of importance. Singh *et al*. (2019) have presented a detailed analysis of 2-2 lobed Roots blower, while operating at low-speed conditions. PIV data of the flow in working chamber was used to evaluate the numerical model. In their study, the rotor grids that were used consisted of fixed nodes on the profile and rotating plus sliding nodes on the housing and the non-conformal interface between the two rotors, called as rotor-to-casing topology (Rane, 2017b). Kennedy *et al.* (2017) have used 1D thermodynamic chamber models and 3D CFD models for the analysis of an oil-free twin screw compressor. An extensive test data of the compressor performance was used for the validation of these models. Eettisseri *et al.* (2021) have analysed heat transfer mapping inside a reciprocating hermetic compressor by considering the rotation of crankshaft and associated motion of connecting rod and piston in a CHT model with Immersed Solid Method in the ANSYS CFX solver. Dincer *et al.* (2017) have presented a non-isothermal CFD analyses of a hermetic reciprocating compressor by means of evaluating the CHT in steady and transient models. In centrifugal compressors, CHT studies are a common design analysis practice, and several studies are available in literature (Gu *et al.*, 2015, Moosania and Zheng, 2016, Roclawski *et al.*, 2016, Stahl *et al.*, 2019). However, in case of positive displacement machines such as twin-screw compressors or Roots blower, detailed CHT analysis are challenging due to the fully transient requirement of the models (Patel, 2022). Yan *et al.*, (2017, 2018) have analysed liquid and multiphase twin screw pump application using CFD

models based on deforming grid principles. EDT – 900 vacuum pump is of twin screw rotor design as shown in Figure 1. The positive displacement principle of compression is used to create a high pressure ratio between the vacuum intake flange and the exhaust flange. The Gate rotor is driven by the drive motor and a timing gear drives the Main rotor. Since these pumps are designed for mobility applications, the exhaust is usually at atmospheric conditions. Through the main AI (air injection), Top AI and Gate AI, additional intake air at atmospheric conditions is provided, thereby allowing cooling to the machine, which permits extended operation at extreme vacuum pressure (Akhtar and White, 2023). The rotary screw nature of the pump with transmission timing gears allows operation without additional lubrication with the additional intake air ensuring that thermal expansion will not disrupt the tight tolerances of the mechanism. The arrangement allows simultaneous operation of the unit as a vacuum pump and air compressor.

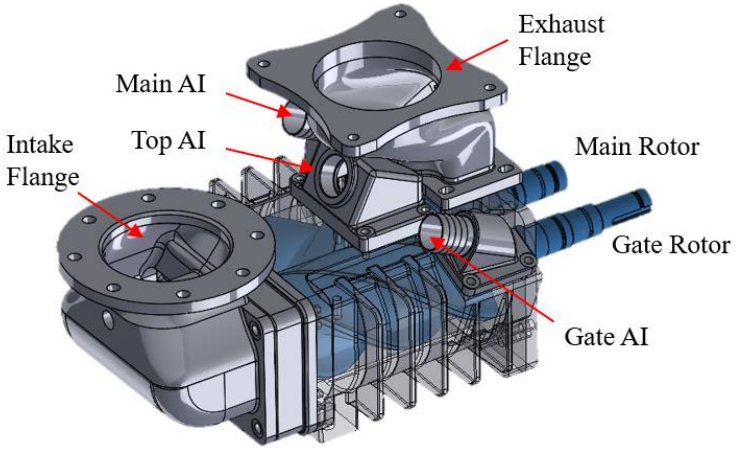

Figure 1: EDT – 900 twin screw vacuum pump with an air injection cooling system

In the present numerical study, the goal was to develop a full transient CFD model of the vacuum pump with air intakes and use some of the available experimental data for the calibration of the model. Such a calibrated CFD model would then be used to investigate the impact of thermal mixing of gas streams and heat transfer phenomenon on rotor cooling and thereby improve the design and performance of the machine. Analysis was carried out in two phases. In Phase I, a CFD Model was successfully developed, and leakage gap were calibrated. CFD performance was calculated at test condition without AI cooling and with AI cooling for comparison and the mechanism of cooling was analysed. In Phase II, design modifications were evaluated. Two variations to the AI ports were: AI opening moved from 170 degree to 240 degree and AI opening width on the Top and Gate side increased from 7.94 mm to 12 and 15 mm, respectively. With these modifications, a 60°C lower exhaust temperature was achieved which is about 10°C better cooling compared to the Base Case. The developed model will be further used to redesign the high-pressure ports and air injection system to improve the thermal cooling effectiveness and specific power of the machine.

2. METHODOLOGY

A test condition of the prototype was available as a guideline and it was aimed to analyse design changes before manufacturing any new prototypes. Since the objective of the study was to evaluate the impact of air intake design changes on the thermal performance of the vacuum pump, it was required to develop a complete 3D transient CFD model of the unit. CHT although an important element of a thermal model, was not included to reduce the complexity and computational size of the model. The study was conducted in two phases.

2.1. Phase I – Evaluation of the test case operating conditions

In Phase I, some of the available test data was used to calibrate the flow estimated by the base CFD model. Base CFD model was generated with design clearance gap sizes. However, due to thermal deformation during operation, these gaps get changed and thus the leakage estimated by CFD model is severely affected. Table 1 indicates the pressure and temperature set for the vacuum pump during the test. These conditions serve as the boundary conditions for the CFD model.

Table 1: Vacuum pump test conditions for CFD model

Boundary	Condition	Specification
Intake	Pressure, Temperature	0.2 bar, 25°C
Exhaust	Pressure	1.0 bar
Main, Gate, Top AI	Pressure, Temperature	1.0 bar, 25°C
Main Rotor	Angular Speed	4200 rpm
Gate Rotor	Angular Speed	2520 rpm

In Phase I, three cases were evaluated. Case 1 is the pump operating with all the air intakes closed (Off). This is a representative condition of a classical twin screw compressor that has been used under vacuum condition and gives an estimate of the base performance of the machine. Design clearances of 40 µm were applied to the interlobe, and radial leakage gaps in this case. Case 2 is an evaluation of the machine under same operating conditions, with all the air intake ports fully open to conditions as indicated in Table 1. In this case the gap sizes were retained at design size. In the Case 3, the gap sizes were reduced to a very low value of 5 µm, such that the resultant gas flow through the pump is closer to that observed in Case 1. This case serves as a comparison of the impact of thermal mixing of intake air on the rotor.

2.2. Phase II – Evaluation of the air intake design parameters

Some design alterations that could improve the cooling effectiveness were identified from Phase I of the analysis:

- Maintain good sealing and lower the leakage to reduce backflow re-heat.
- Vacuum and exhaust pressure condition needs to be separated by at least one chamber.
- Maximise the metal surface of each lobe that interacts with AI flow before re-compression.
- Minimise connection block volumes.

Due to tight product roll out schedules, design was constrained on the extent of changes that could be implemented. Namely, they were limited to modification of just the AI port design (timing and sizing). Other parameters that were potentially better for a thermal performance improvement of the pump, such as rotor wrap angle, rotor profile and design were constrained to its current specification. The control parameters of the air intake system are the timing of connection of the port with the pumping cycle and the size of the opening that allows the external flow to be connected. The original design indicated as Base Case in Figure 2 was timed on the rotor wrap angle and cut-off of the suction port. Base Case was than modified in Phase II. P2-Case 1 shown in Figure 2 has a delayed timing of connection but same size of the port area. This delay allows for more than one rotor lobe to act as a separator between the exhaust and suction pressure difference. Table 2 provides the port timing setup of this modification. P2-Case 2 in Figure 2 is a delayed connection timing together with a larger size of the Top and Gate air intake areas, as indicated in Table 2. This larger area could potentially introduce a balanced cooling flow and provide better thermal mixing.

Table 2: Phase II design parameters

Phase II	Parameter	Base Condition	Modification	Scope
P2-Case1	AI opening	170 degree	240 degree	Two lobe spacing between vacuum and AI openings – reduce leakage and power rise
P2-Case2	Main AI	7.94 mm	No change	Reference cooling flow
	Gate AI	7.94 mm	15 mm	Increase the cooling flow
	Top AI	7.94 mm	12 mm	Increase the cooling flow

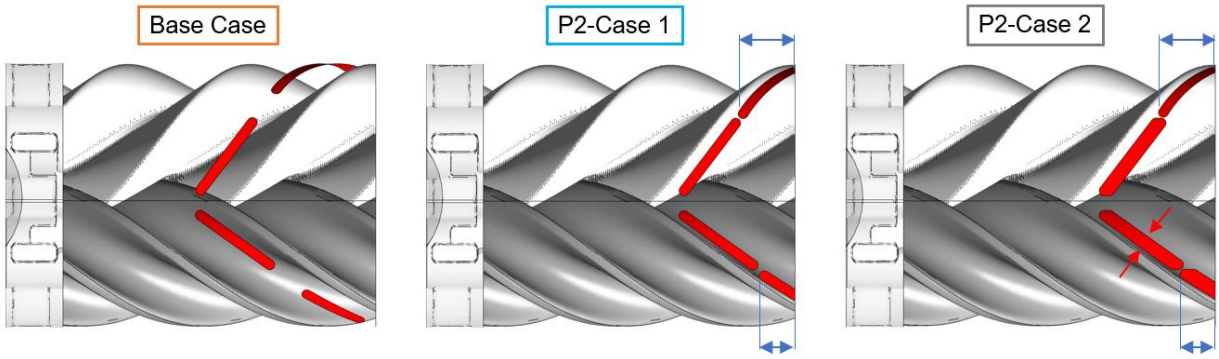

Figure 2: Design modification of the air injection system, Red – Port area

3. CFD MODEL

The computational model for positive displacement machines such as twin-screw compressors has been described in Kovačević (2005, 2007) and is widely applicable, such as for the presented vacuum pump model. Rane (2017a, 2017b, 2021a) and Kovačević (2017) have presented the development and application of different types of deforming grid topologies that can be used for modelling of twin-screw machines. Figure 3 shows the main components of the CFD model developed in this study. The goal of the CFD model was to evaluate the impact of air intake design changes on the thermal performance of the vacuum pump.

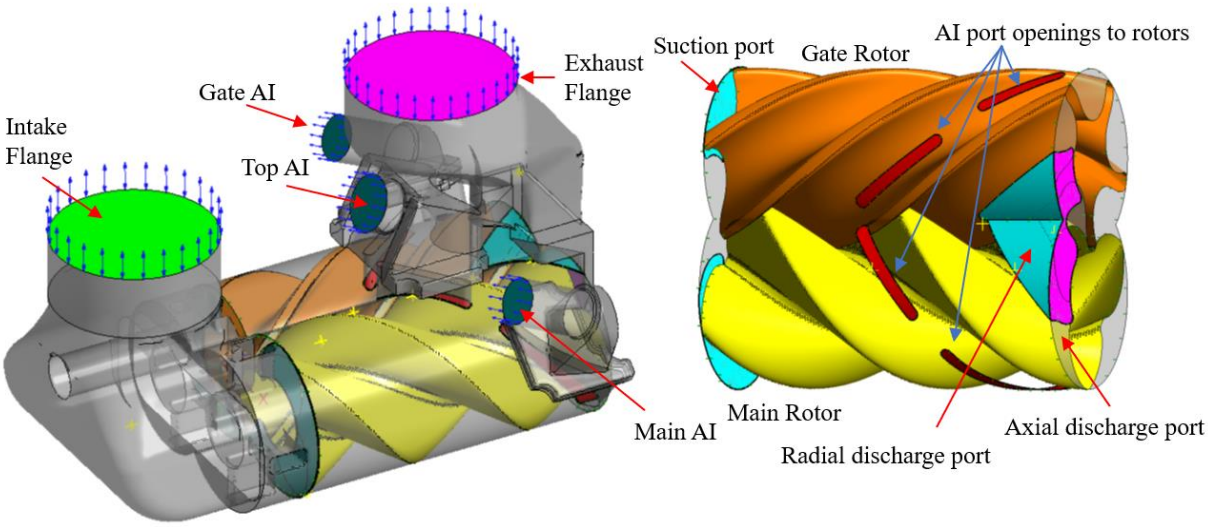

Figure 3: Components of the numerical model – fluid domains, boundaries and air intake ports

As shown in the Figure 3, the fluid domains were extracted from the CAD model of the pump and split into several components. The Intake flange is located on the suction domain at vacuum conditions as specified in Table 1. The suction domain has the area of the Suction port. Main and Gate rotors are both contained in the rotor domain and are connected to the other components through fluid-fluid interfaces. The rotor domain is also a deforming grid and changes shape during the CFD simulation. Exhaust flange is located on the discharge domain. Discharge is made up of radial and axial port areas. These interface with the rotor domain and determine the built-in volume change of the machine. There are three AI ports in the prototype EDT – 900 pump, on the Main side, on the Top and on the Gate side respectively. These AI ports have slots of rectangular helical shape as shown in Figure 3. Each AI port has its opening boundary condition as specified in Table 1 and the helical areas interface with the rotor domain. Interlobe and radial leakage gaps are present within the deforming rotor grid and remain constant as CHT and thermal deformation has not been included in this model.

3.1. Grid Generation

SCORG grid generator (Kovačević and Rane, 2017) was used for the deforming rotor grid generation and ANSYS meshing tools were used for the stationary fluid domains as well as the air intake ports. A hexahedral cell structure as shown in Figure 4 is preferred in the deforming rotor domain. Other components have a combination of hexahedral and tetrahedral cell structure in order to conform with the geometry of the ports and the pump housing. A casing-to-rotor type conformal rotor grid with a single domain for both the rotors was used.

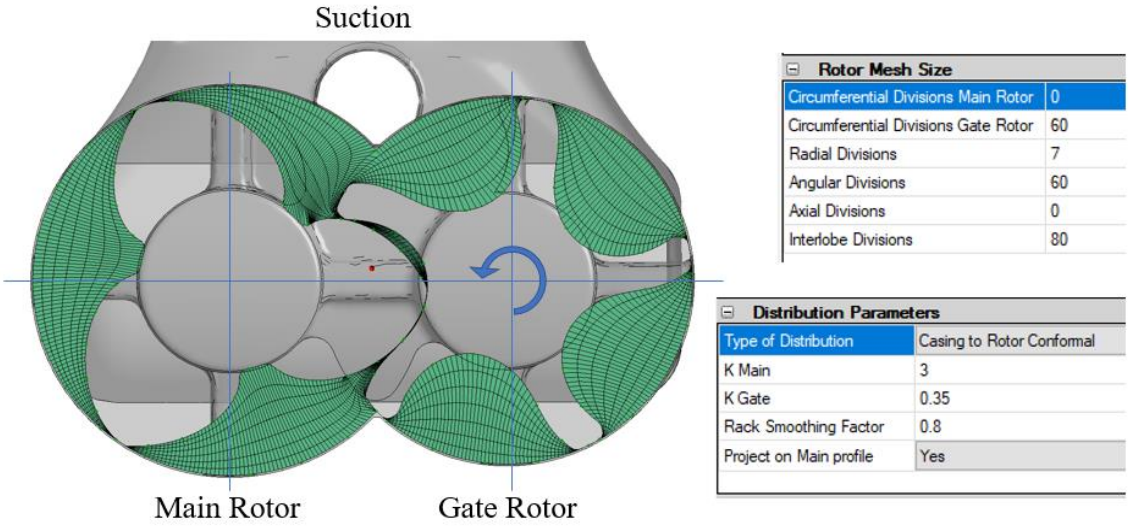

Figure 4: Deforming rotor domain grid generated using SCORG

On the rotor profiles a node density of 60 per lobe was specified. Radially, a 7 division spacing and an angular discretization of 2 degree per step was specified. As a result, the total node count in the deforming rotor domain was 726880. In the stationary fluid domain, it was 130217, in the suction domain 65546, air intake ports 37330 and in the discharge domain it was 27341. The whole CFD model size was thus close to 857097 nodes.

Table 3: Air properties specification for the model

Material	Density	Dynamic Viscosity	Thermal Conductivity	Specific Heat
Air	Ideal Gas Law	1.831E-05 kg m^{-1} sec^{-1}	0.0261 W m^{-1} K^{-1}	1004.4 J kg^{-1} K^{-1}

3.2. Numerical Solver

ANSYS CFX which is a well validated CFD solver in the application of positive displacement machines was used in the current study. Singh *et al.* (2020) have used the same solver in their PIV based investigation of a dry air Roots Blower. Table 3 provides the specification of air properties used in the model setup. Since the vacuum suction pressure is about 0.2 bar absolute, it is suitable to use the standard Finite Volume Method based numerical solver and define the gas as Ideal gas law. Table 4 provides the specification of the important parameters of the numerical solver. Operating speed of the Main rotor was 4200 rpm and this together with the grid transition of 2 degree per time step was used to specify the time step size of 7.93651e^{-5} sec to the solver.

Table 4: Specification of the numerical setup in the ANSYS CFX solver

Rotor mesh deformation	User defined nodal displacement	Advection scheme	High Resolution
Mesh in ports	Tetrahedral with boundary layer refinements (ANSYS Mesh)	Transient scheme	Second order Backward Euler
Turbulence model	SST – k Omega (Standard Wall Functions)	Transient inner loop coefficients	10 iterations per time step
Inlet/Supercharge boundary condition	Opening (Specified total pressure and temperature)	Convergence criteria	r.m.s residual level 1e^{-03}
Outlet boundary condition	Opening (Static pressure, backflow acts as total pressure and temperature)	Relaxation parameters	Solver relaxation fluids (0.1)

4. RESULTS AND DISCUSSION

Each case was calculated for sufficient number of flow cycles that resulted in a cyclic variation of the performance parameters. The data for internal pressure and temperature variation together with the main operating performance such as indicated power, vacuum flow, AI flows was collected from the model. These results were used to evaluate the impact of AI port design and its modification on the thermal performance of the pump.

4.1. Performance results

Table 5 presents the performance results from the Phase I and Phase II conditions. Case 1 is the base design operated with AI cooling ports Off and a design gap. This was achieved by deactivating the AI inlet boundary conditions. Case 2 is the same gap size with AI intake turned On. Case 3 is a reduced gap size and AI intake turned On. This case is also referenced as Base Case in Phase II evaluation and has a AI port timing of 170 degree. P2-Case 1 is a delayed AI port timing to 240 degree and P2-Case 2 is further design modification to increase the Top and Gate AI slot area. As indicated in Table 5, the main rotor speed was set at 4200 rpm in all the cases. Vacuum temperature and Outlet temperature data are the cyclically averaged gas temperature at the rotor inlet and exhaust respectively. From Table 5, Case 1 shows that when the AI ports are not engaged, a vacuum flow through the machine is 0.563 kg/min. Internal peak pressure is slightly above the exhaust at 1.09 bar. The indicated power of the pump is 6.18 kW. A vacuum temperature of 37℃ and outlet temperature of 105℃ is seen. Case 2 indicates that when AI ports are opened, the flow through the ports starts. The peak internal pressure increases to 1.14 bar and net vacuum flow is not positive (high leakage). This results into a significantly high vacuum temperature of 65℃. Such a model cannot be used for design tests as the results will be insensitive to AI port modifications. Further Case 3 improves the situation with a net vacuum flow close to Case 1. In this condition the peak internal pressure is same as Case 2 resulting into a high indicated power of 10.44 kw (4.27 kW higher than Case 1). Vacuum temperature of 36℃ and outlet temperature of 55℃ is seen. This is nearly 50℃ cooler than Case 1 due to thermal mixing of the main flow with the AI cooling flow streams.

Table 5: Evaluation of the Phase I and II conditions

	Cooling Condition	Gap size	Vacuum Pressure	Speed	Vacuum flow	Cooling flow			Peak pressure	Power	Vacuum temperature	Outlet temperature
		[µm]	[bar]	[rpm]	[kg/min]	[kg/sec]	[kg/sec]	[kg/sec]	[bar]	[kW]	[°C]	[°C]
						Main	**Top**	**Gate**				
Case 1	Closed	40	0.2	4200	0.563	0	0	0	1.09	6.18	37.05	105.23
Case 2	Full Open	40	0.2	4200	0	0.034	0.024	0.012	1.14	10.16	65.46	58.46
Case 3 Base Case	Full Open	5	0.2	4200	0.453	0.034	0.024	0.012	1.15	10.44	35.99	55.21
							Difference: Case 3 and Case 1			**4.27**		**50.02**
P2-Case1	Full Open	5	0.2	4200	0.892	0.029	0.038	0.011	1.14	7.93	25.18	43.72
P2-Case2	Full Open	5	0.2	4200	0.906	0.028	0.041	0.011	1.14	7.96	27.67	42.13
							Difference: P2-Case 1 and Case 1			**1.75**		**61.51**

Phase II cases are compared with Case 3 as the Base Case. In P2-Case 1 the timing of AI port opening is delayed by one interlobe space. A high resultant vacuum flow of 0.892 kg/min was seen with this change. The peak internal pressure is of the same level as Base Case (Case 3 in Table 5), however, the indicated power is 7.93 kW. This is only 1.75 kW higher than the Base Case. At vacuum temperature of 25°C, the outlet temperature observed is about 44°C. Similarly, P2-Case 2 shows a further higher vacuum flow of 0.906 kg/min. For the same peak pressure, the indicated power is 7.96 kW. For a vacuum temperature of 28°C, the outlet temperature is about 42°C. These observation suggest that AI port design changes have resulted into a better sealing and cooling effectiveness.

An analysis of the AI flow indicates that in the Base Case there is a large imbalance between the Main, Top and Gate flows. Their cyclic average being in the proportion 3:2:1 respectively. With design modification, the Main flows showed a decrement while the Top flows showed a greater than 50% increment. Further analysis of the pressure and temperature variations is discussed in the next sections and can be corelated with the data in Table 5.

4.2. Internal gas pressure distribution

A comparison of the pressure distribution between Case 1 and Case 3 is shown in Figure 5. Pressure cycles indicate a vacuum level of 20 kPa and an exhaust at 100 kPa. The connection blocks at 40 kPa suction. Connection blocks were confirmed to be disconnected from vacuum and exhaust (small angle) i.e. no direct leak. In Case 1, after suction closure, an intermediate pressure of 40 kPa is seen in the chamber. After discharge ports open, chamber pressure sharply rises to 100 kPa. In Case 3, vacuum and exhaust pressure conditions get separated effectively by just one flute (120 degree). Following the opening of the AI ports, an internal over-compression to 120 kPa occurs and this results into heavy leakage. Pressure vs Angle variation's shaded area represents the increase in indicated power. Indicated power of the pump increases by 70% in Case 3 as seen in Table 5 .

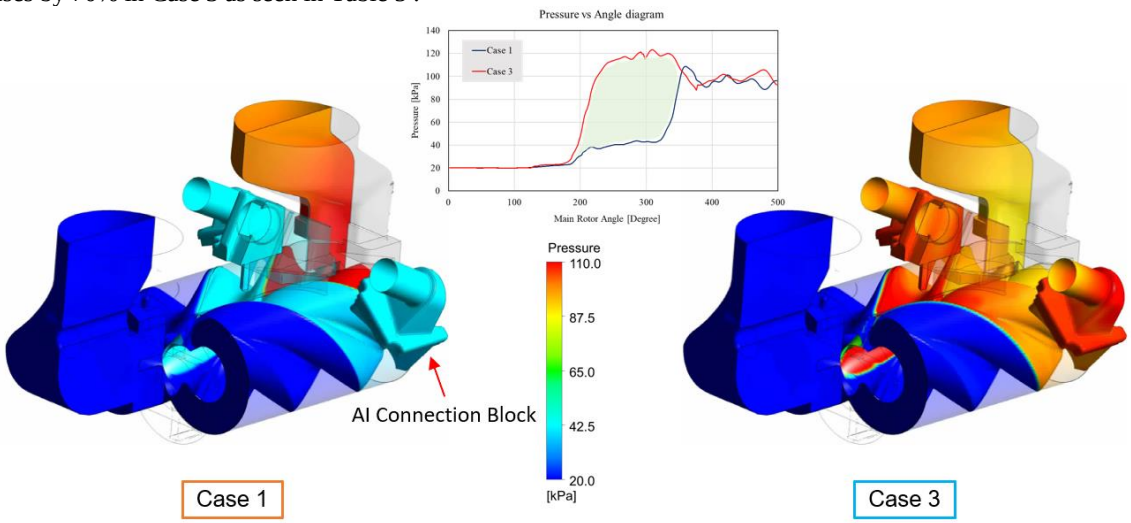

Figure 5: Evaluation of pressure distribution in Phase I cases, Case 1 – Cooling Off, Case 3 – Cooling On

A comparison of the pressure distribution between Base Case and P2-Case 1 is shown in Figure 6. In the Base Case, AI ports get connected to chamber at 170 degree. While in the P2-Case 1, AI ports get connected to chamber at 240 degree. Pressure vs Angle variation's area represents an increase in indicated power compared to Case 1 and is lower than the Base Case. In P2-Case 1, vacuum and exhaust pressure conditions get separated by two flutes (240 degree) as desired. Following the opening of the AI ports, an internal over-compression to 114 kPa occurs which in comparison was 120 kPa in the Base Case. Thereby, a relatively lower leakage and increase in indicated power of the pump by 30% is seen in this case (Table 5).

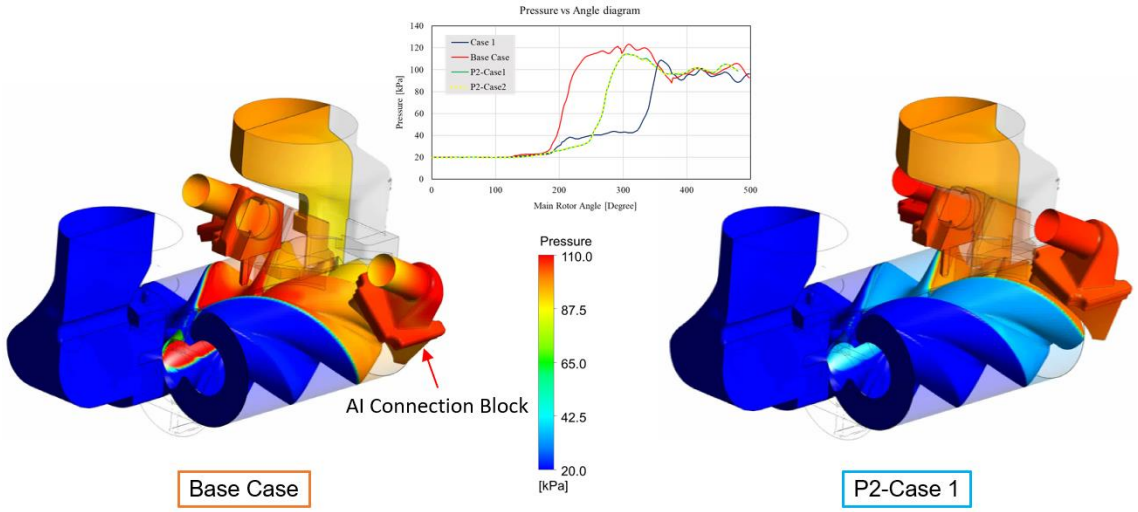

Figure 6: Evaluation of pressure distribution in Phase II, Base Case – 170 deg, P2-Case 1 – 240 deg timing

4.3. Internal gas temperature distribution

A comparison of the gas temperature distribution between Case 1 and Case 3 is shown in Figure 7. Temperature cycles from Case 1 shows a high exhaust temperature above 100°C. Whereas, Case 3 with Cooling On shows 50°C lower exhaust temperature. In Case 3 there is a large imbalance seen between the Main, Top and Gate AI flows (Table 5). A point inside the rotor domain marked as P7 is located near the Main AI slot before exhaust port is opened. This point represents the peak temperature during the operation of the pump. It is seen that in Case 1 the P7 temperature cycle to a maximum of 115℃ and in Case 3, it cycles to a maximum of about 60℃. The vacuum temperature in both cases is around 35℃. The analysis confirms the working of the cooling ports. Though, gas mixing causes certain level of cooling in exhaust, it is not effective in dissipating full heat from the rotors, especially the vacuum side.

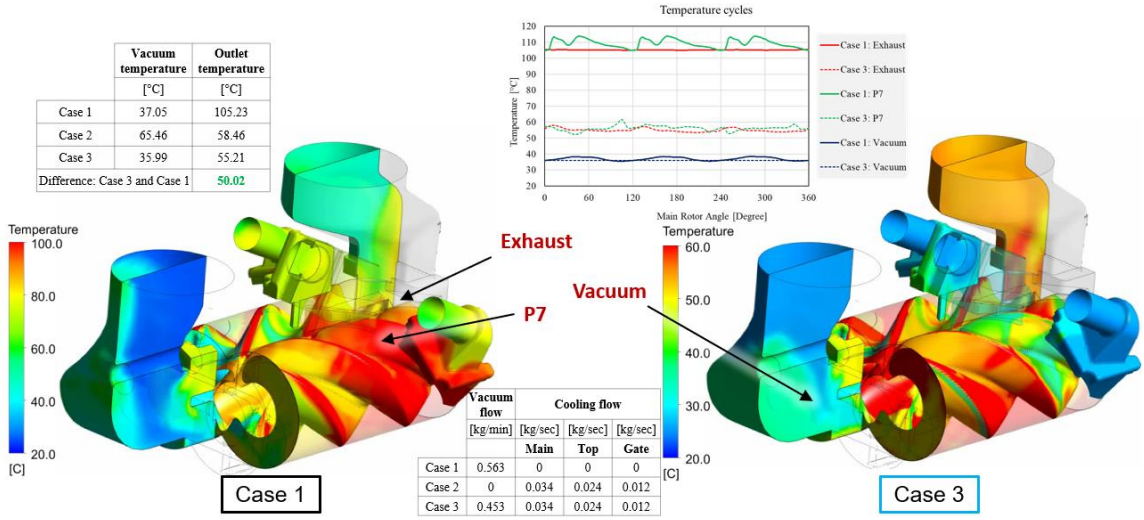

	Vacuum temperature	Outlet temperature
	[°C]	[°C]
Case 1	37.05	105.23
Case 2	65.46	58.46
Case 3	35.99	55.21
Difference: Case 3 and Case 1		50.02

	Vacuum flow	Cooling flow		
	[kg/min]	[kg/sec]	[kg/sec]	[kg/sec]
		Main	Top	Gate
Case 1	0.563	0	0	0
Case 2	0	0.034	0.024	0.012
Case 3	0.453	0.034	0.024	0.012

Figure 7: Evaluation of gas temperature in Phase I cases, Case 1 – Cooling Off, Case 3 – Cooling On

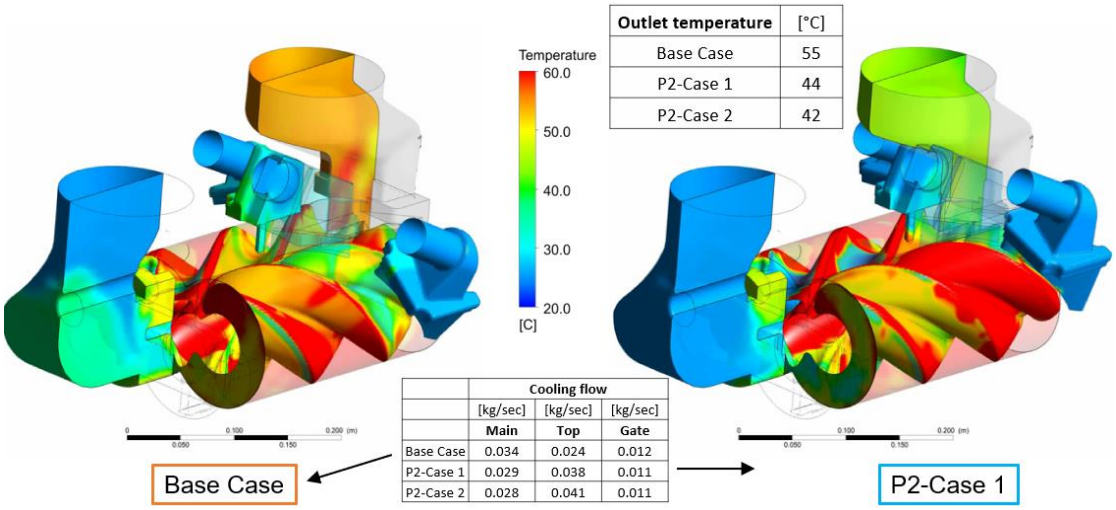

Figure 8: Evaluation of gas temperature in Phase II, Base Case – 170 deg, P2-Case 1 – 240 deg timing

A comparison of the gas temperature distribution between Base Case (Case 3 of Phase I) and P2-Case 1 is shown in the Figure 8. In the Base Case, AI ports get connected to chamber at 170 degree. While in the P2-Case 1, AI ports get connected to chamber at 240 degree. In the Base Case, exhaust temperature reaches 55°C. It should be noted that for gas temperature results, it is important to study relative changes between each case, as the absolute temperature recorded on the pump will be a result of many additional contributions such as frictional heat dissipation. In the P2-Case 1, exhaust temperature reaches 44°C and in the P2-Case 2, it reaches 42°C. Thus, a 10-12°C better cooling can be seen from these design modifications. In both cases the vacuum temperature is about 26°C indicating a better sealing of the leakage flow. Flow through the AI's was still found to be imbalanced (Table 5). This was due to the shortened length on Main and Gate side. Top AI flow increased, Main AI flow reduced, and Gate AI flow was nearly the same.

4.4. Air intake port flow

The geometry of the AI ports consists of tubular intakes joining the connection blocks. The connection blocks have a relatively larger volume than these tubular intakes. A cyclic variation of flow data at the intake of the main AI port and at the interface between the rotor and the helical slot is presented in Figure 9 for one rotation of the main rotor. Three flow cycles can be seen in both the data. There is also a phase lag between the flow entering the AI intake and the flow entering the main rotor. This lag is due to the volume of the connection block.

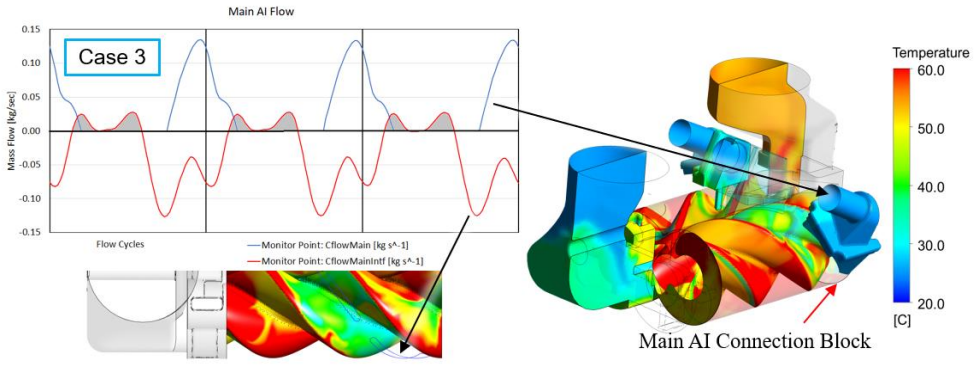

Figure 9: Flow characteristics of the air intake ports – Case 3 (Base case)

Under ideal flow connection the cold gas must enter the rotors through the helical slot and get added to the pump's main flow cycle. However, as seen in Figure 9, there is a flow reversal or back-flow happening in each cycle. The magnitude is marked by the grey area. Cold gas enters the rotor domain which is under vacuum pressure at that time. Rapidly, pressure difference between the rotor chamber and the AI port reduces and a flow pulsation is observed. The cold gas has mixed with hot gas in the rotors and a fraction of this hot gas is pushed back into the connection block volume. It remains accumulated there and enters the rotor chamber in the next cycle, thereby reducing the net

amount of new volume of cold gas that could enter the rotors. This nature of the air intake flow lowers the effectiveness of the cooling system. A redesign of the connection blocks, such that the AI cooling stream is prevented from experiencing a back-flow could help in lowering the inefficient intake process.

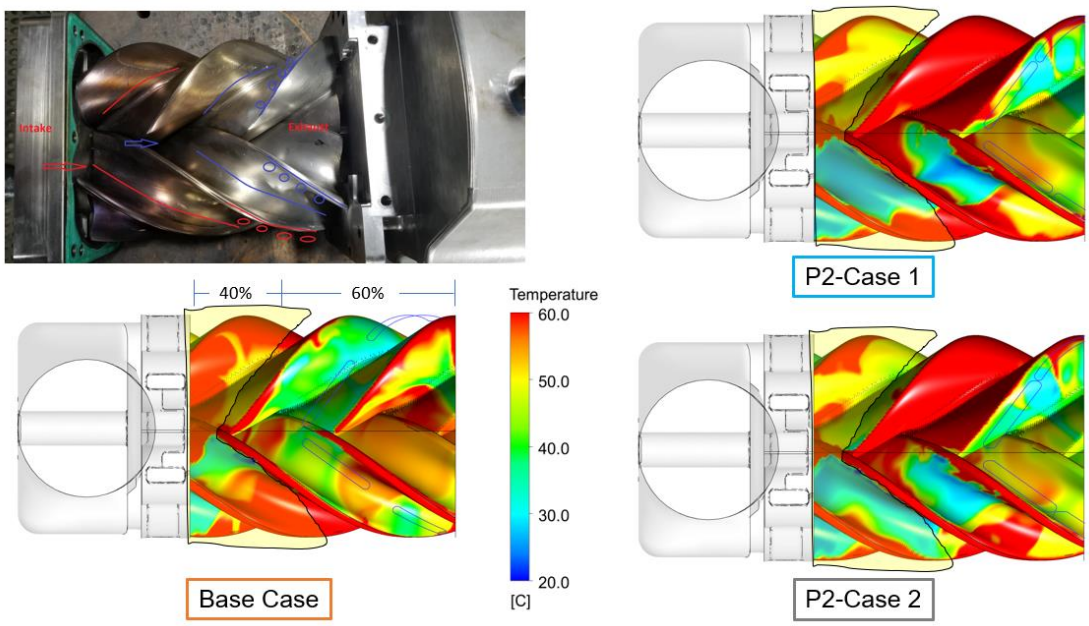

Figure 10: An image of the rotor surface and comparison of temperature distribution

4.5. Rotor temperature evaluation

EDT – 900 pump was initially designed with a screw rotor profile that featured a relatively large blow hole area. Testing of the prototype showed poor extended operation ability of the machine with a high resultant temperature of the housing. After the prototype's internal parts were evaluated, rotor surface discoloration due to exposure to high temperature was observed, as shown in Figure 10. The intake end of the rotors that are connected to vacuum condition showed severe discoloration as compared to the end connected to the AI ports and the exhaust. Figure 10 presents a comparison of the rotor temperature in the Base case and with the Phase II design modification. These results are on an upgraded rotor profile with reduced blow hole area and better extended operation ability. In the Base Case, an area marked by about 40% rotor length indicates that the intake end of the rotors is at high temperature. This area corresponds to the discoloration observation from test rotors and confirms the finding from the CFD model that cooling flow is isolated from the 40% rotor space. As a result, high exhaust temperature of 55℃ was seen in the Base case (cooling on) as indicated in Table 5. It is also seen that recompression of the AI flow starts as soon as the suction port is passed by the rotors. In comparison, both Phase II cases have shown a better cooling in this 40% rotor space connected to vacuum condition. The difference between P2-Case 1 and P2-Case 2 at these local conditions is very small, with P2-Case 2 showing better gate rotor cooling area. This is due to the large Top slot area in this design. In Table 5, both P2 cases have an increase in the Top AI flow and a lower exhaust gas temperature by about 10℃, thus giving an improved cooling performance.

5. CONCLUSIONS

The objective of the study was to evaluate the impact of air intake design changes on the thermal performance of the vacuum pump. Analysis was carried out in two phases. In Phase I, a CFD Model was successfully developed, and leakage gap were calibrated. SCORG tool was used for rotor grid generation. CFD performance was calculated at test condition without AI cooling and with AI cooling for comparison and the mechanism of cooling was analysed.

- Flow through AI's are timed after closure of suction and before the discharge port opens. This was confirmed from the CFD results. Cyclic flow through the three AI's was found to be imbalanced.
- When AI were open 50°C lower exhaust temperature was achieved. However, indicated power increased by 70% due to resultant chamber pressure rise. Over-compression and peak pressure above the exhaust was observed when AI were open which is detrimental to the pump's performance.

- Though, gas mixing causes certain level of cooling in exhaust, it is not effective in dissipating full heat from the rotors, especially the vacuum side.

In Phase II, design modifications were evaluated. Two variations to the AI ports were: AI opening moved from 170 degree to 240 degree and AI opening width on the Top and Gate side increased from 7.94 mm to 12 and 15 mm, respectively.

- With these modifications, 60°C lower exhaust temperature was achieved which is about 10°C better cooling compared to the Base Case.
- Increase in vacuum flow indicated a lower leakage with the Phase II design. Flow through the AI's was still found to be imbalanced. This was due to the shortened length on Main and Gate side. Top AI flow increased, Main AI flow reduced, and Gate AI flow was nearly the same.
- Indicated power increased by 30% due to pressure rise. In the Base Case, this increase was substantially high at 70%.
- In the Base Case, over 40% surface of the rotors from vacuum side were not contacting cold flow. With Phase II modifications, better cooling was seen in this region.

Based on the improved results, it was recommended to move the AI opening from 170 degree to 240 degree. Further design improvements were also identified. Either by increasing the wrap angle or redesign of the rotor with higher number of lobes, the pressure diffusion can be made more gradual. This will increase the effectiveness of the cooling flow through AI ports and potentially lower the indicated power consumption of the pump.

REFERENCES

Akhtar, K. & White, C. (2023), Cooled dry vacuum screw pump. US patent number 11708832 B2.

Dincer, M., Sarioglu, K. & Gunes, H. (2017). A conjugate heat transfer analysis of a hermetic reciprocating compressor. 10th Int Conf on Compressors and their Systems, London. IOP Conf. Ser.: Mater. Sci. Eng. 232 012010

Eettisseri, R., Real, M., & Oliveira, S. (2021). Analysis Of Dynamic Heat Transfer Coefficient In a Reciprocating Compressor By Immersed Solid Method in CFD. Int Compressor Engineering Conference. Purdue. Paper 2653.

Gu L., Zemp A. & Abhari R. (2015). Numerical study of the heat transfer effect on a centrifugal compressor performance. Proc IMechE Par t C: J Mechanical Engineering Science 2015, Vo l. 229(12) 2207–2220.

Kennedy, S., Wilson, M., & Rane, S. (2017). Combined Numerical and Analytical Analysis of an Oil-free Twin Screw Compressor. IOP Conf. Ser. Mater. Sci. Eng. 232, 012080.

Kovačević, A. (2005). Boundary Adaptation in Grid Generation for CFD Analysis of Screw Compressors, *Int. Num. Eng*., 64(3), 401-426.

Kovačević, A., Stošić, N. & Smith, I. K. (2007). *Screw compressors - Three dimensional computational fluid dynamics and solid fluid interaction*, ISBN 3-540-36302-5, Springer-Verlag Berlin Heidelberg New York.

Kovačević, A. & Rane, S. (2017). Algebraic generation of single domain computational grid for twin screw machines. Part II. Validation, *Advances in Engineering Software*, 109, 31-43. doi.org/10.1016/j.advengsoft.2017.03.001

Moosania, S. M. & Zheng, X. (2016). Comparison of Cooling Different Parts in a High Pressure Ratio Centrifugal Compressor. MDPI, Appl. Sci., 7, 16; doi:10.3390/app7010016

Patel, B., Rane, S., & Kovacevic, A. (2022). Infrared-Thermography and Numerical Investigation Of Conjugate Heat Transfer In Roots Blower. Int Compressor Engineering Conference. Purdue. Paper 2709.

Rane, S. & Kovačević, A. (2017a). Application of numerical grid generation for improved CFD analysis of multiphase screw machines, 10th International conference on compressors and their systems, London, IOP Conf. Ser.: *Mater. Sci. Eng.*, 232, 01. DOI:10.1088/1757-899X/232/1/012017

Rane, S. & Kovačević, A. (2017b). Algebraic generation of single domain computational grid for twin screw machines. Part I. Implementation, *Advances in Engineering Software*, 107, 38-50. doi.org/10.1016/j.advengsoft.2017.02.003

Rane, S., Kovačević, A., Stošić, N. & Smith, I. (2021a). Analysis of real gas equation of state for CFD modelling of twin screw expanders with R245fa, R290, R1336mzz(Z) and R1233zd(E). *International Journal of Refrigeration*. 121:313-326. DOI: 10.1016/j.ijrefrig.2020.10.022.

Rane, S., Kovačević, A., Stošić, N. & Smith, I. (2021b). Bi-Directional System Coupling for Conjugate Heat Transfer and Variable Leakage Gap CFD Analysis of Twin-Screw Compressors. IOP Conf. Ser.: Mater. Sci. Eng. 1180 012001. doi.org/10.1088/1757-899X/1180/1/012001

Roclawski, H., Oberste-Brandenburg, C. & Böhle, M. (2018). Conjugate Heat Transfer Analysis of a Centrifugal Compressor for Turbocharger Applications. 16th ISROMAC 2016. Honolulu, hal-01884259.

Singh, G., Sun, S., Kovacevic, A., Li, Q. & Bruecker, C. (2019). Transient flow analysis in a Roots blower: Experimental and numerical investigations. Mechanical Systems and Signal Processing, 134, 106305. doi: 10.1016/j.ymssp.2019.106305

Stahl, M., Franz, h. Ittern, L. (2019). Conjugate Heat Transfer Study of a Centrifugal Compressor with Impeller Cavities. Global Power and Propulsion, Zurich. GPPS-TC-2019-0054.

Yan D., Kovacevic A., Tang Q. (2017). Numerical modelling of twin-screw pumps based on computational fluid dynamics. Proceedings of the Institution of Mechanical Engineers, 231(24), pp. 4617-4634.

Yan D., Tang Q., Kovacevic A. (2018). Rotor profile design and numerical analysis of 2-3 type multiphase twin-screw pumps. Proceedings of the Institution of Mechanical Engineers, Part E: Journal of Process Mechanical Engineering, 232(2): 186-202.